Supporting Information

Extending conducting channels in Fe-N-C by interfacial growth of CNT with minimal metal loss for efficient ORR electrocatalysis

Reeya Garg[a], Mohit Jaiswal[a], Kaustubh Kumar[a], Komalpreet Kaur[a], Bhawna Rawat[b], Kamalakannan Kailasam[b], Ujjal K. Gautam[a,*]

[a]Department of Chemical Sciences, Indian Institute of Science Education and Research (IISER)-Mohali, Sector 81, SAS Nagar, Mohali 140306, Punjab, India

[b]Advanced Functional Nanomaterials, Institute of Nano Science and Technology (INST), Knowledge City, Sector-81, Manauli, SAS Nagar, 140306 Mohali, Punjab, India

Corresponding author: ujjalgautam@iisermohali.ac.in, ujjalgautam@gmail.com

Supporting Note 1

The structural identity of the composite catalyst during prolonged cyclic test was tracked by microscopic and spectroscopic analysis of post-ORR samples. The FTIR spectra of both the as-synthesized and post-catalysis of Fe-NPs-N-C/CNT were recorded to analyse the surface chemical entities shown in **Fig. S12a**. The prominent absorption band around 1350 cm^{-1} shows the presence of -C=N moieties originated from graphitic as well as pyridinic nitrogens, also suggested by –C-N stretching peak around 1250 cm^{-1}.[1] There are other bands around 3500 cm^{-1} and 1620 cm^{-1} indicates -OH and carbonyl functionalities[2] respectively, arising either surface oxidation induced by the trace O_2 present in Argon flow used during the synthesis or pre-treatment of commercial carbon performed prior to the synthesis of Fe-N-C. The carbonyl and hydroxyl groups were also suggested by the peaks around 1050 cm^{-1} and 1140 cm^{-1} which corresponds to –C-O (carbonyl) and –C-O (of –C-OH) stretching frequencies respectively. The presence of -CH functionalities[3] are reflected in the band around 2900 cm^{-1} and 600 cm^{-1}. There were no significant changes in the spectra of the sample post-catalysis, as all IR bands persisted with similar intensities. This suggested that there are no changes in surface functionalities of the samples before and after catalysis. Furthermore, we also performed morphological analysis of the post-ORR catalyst and no visual structural change was noticed as shown in **Figure S12b**.

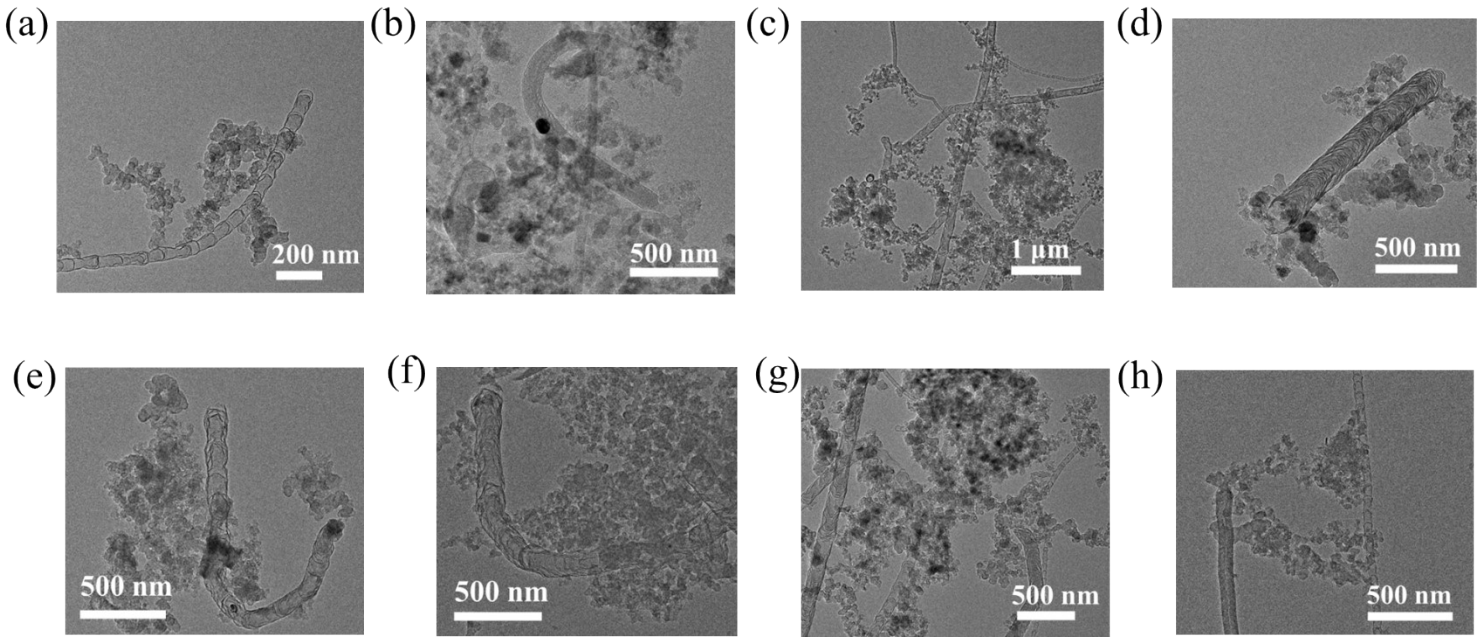

Fig. S1 Additional TEM images of the composite Fe-NPs-N-C/CNT.

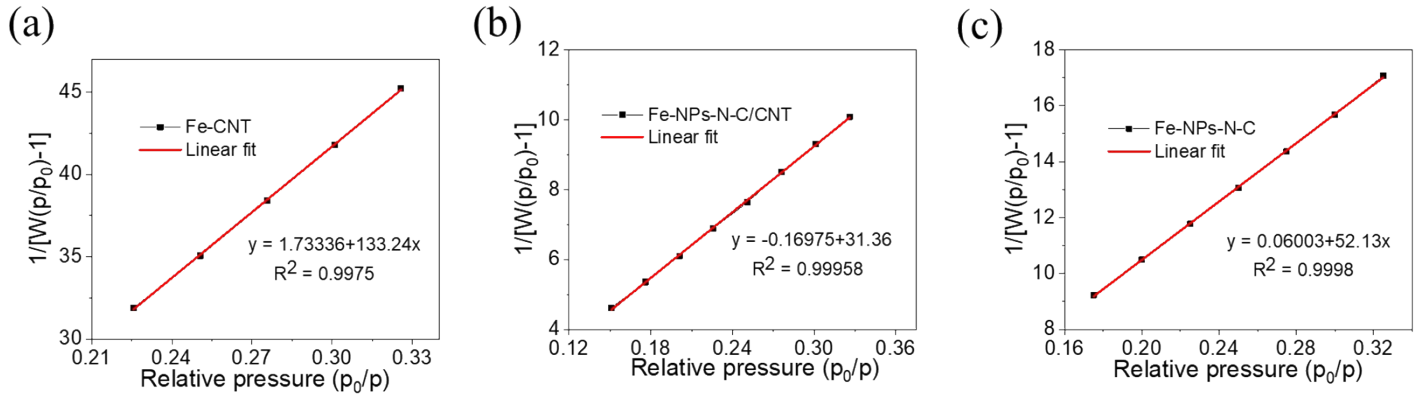

Fig. S2 BET multipoint plots of (a) Fe-CNT, (b) Fe-NPs-N-C/CNT, and (c) Fe-NPs-N-C.

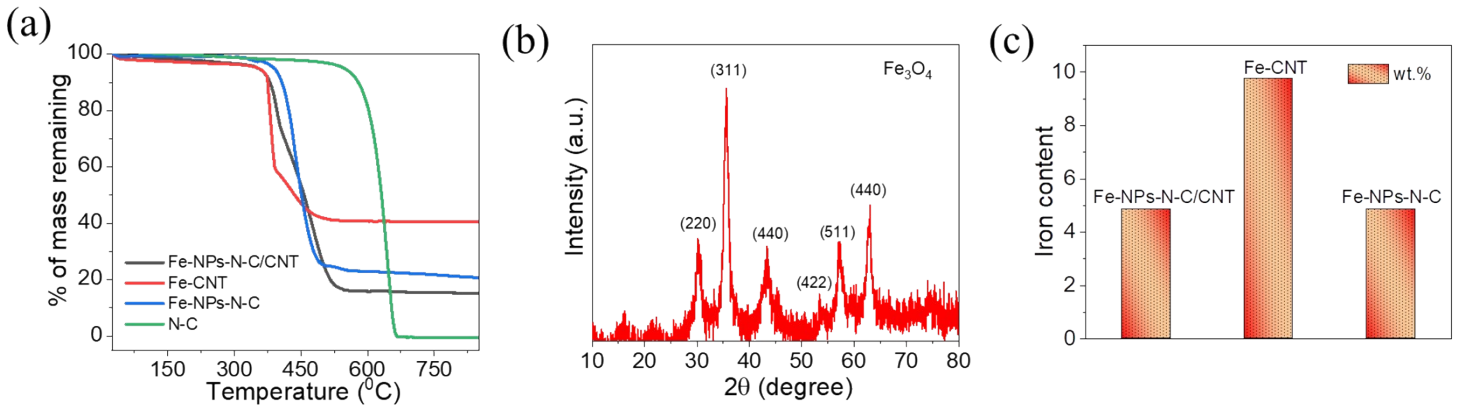

Fig. S3 (a) Thermal gravimetric analysis (TGA) plots of Fe-CNT, Fe-NPs-N-C/CNT, and Fe-NPs-N-C (b) PXRD pattern of the residue collected after TGA, (c) iron content (wt.%) in different samples estimated from TGA analysis.

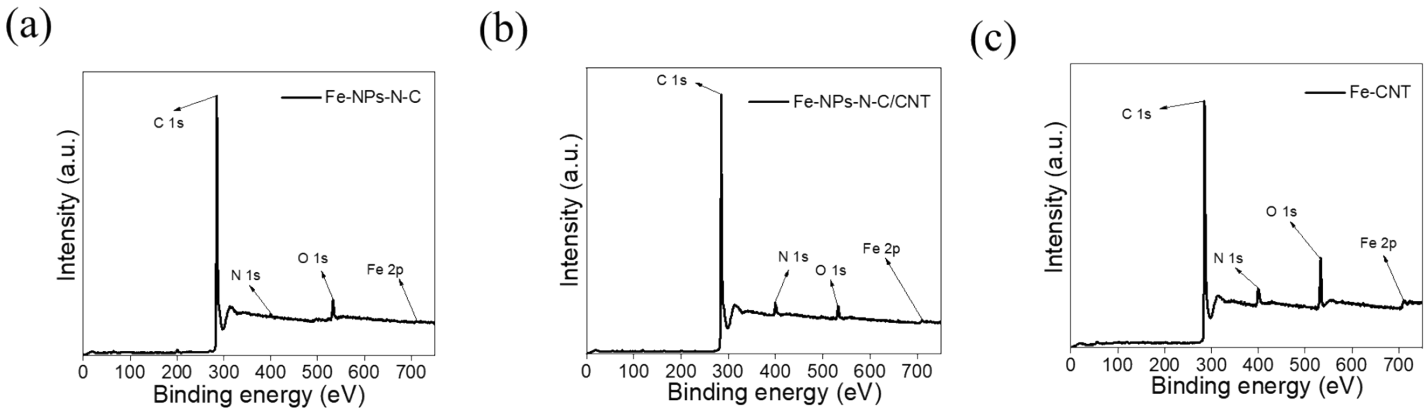

Fig. S4 XPS survey scans of (a) Fe-NPs-N-C, (b) Fe-NPs-N-C/CNT, and (c) Fe-CNT.

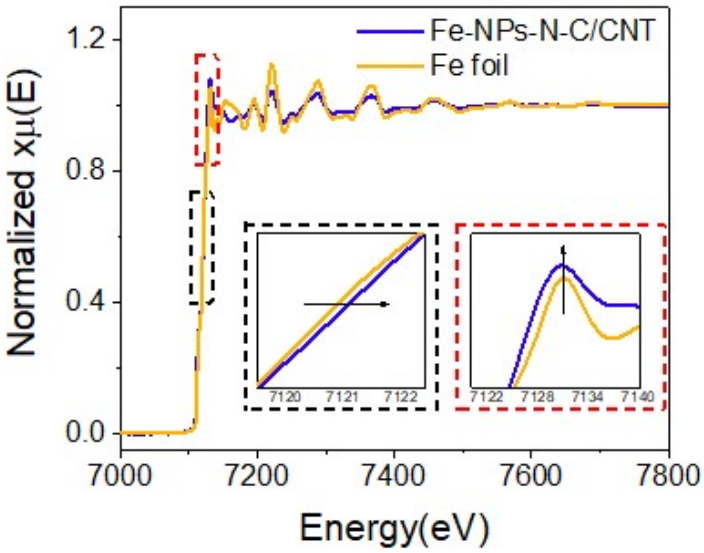

Fig. S5 Fe K-edge of XANES spectra for Fe-NPs-N-C/CNT and Fe foil.

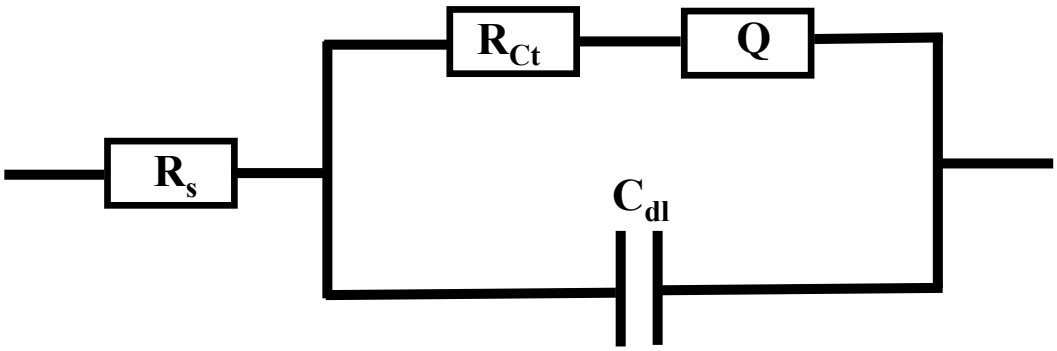

Fig. S6 Randles equivalent circuit used for fitting the experimental impedance measurement data for the Nyquist plots. The circuit consists of solution resistance (R_s), charge transfer resistance (R_{ct}), double layer capacitance (C_{dl}), and a constant phase element (Q).

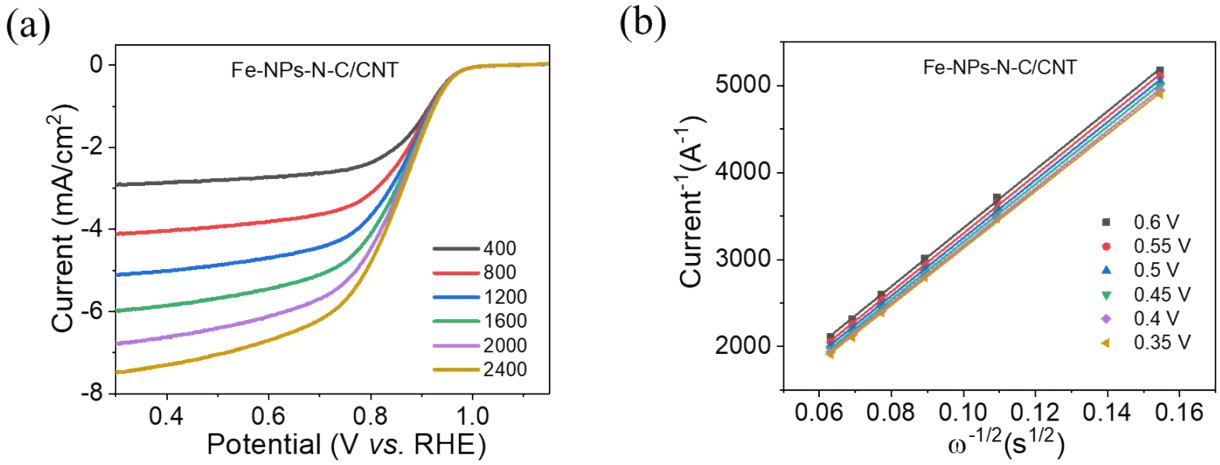

Fig. S7 (a) ORR polarization curves of Fe-NPs-N-C/CNT recorded at different rotation rates in O_2 saturated 0.1 M KOH with a scan-rate of 10 mV/s, b) the corresponding K-L plots at different potentials *w.r.t.* RHE.

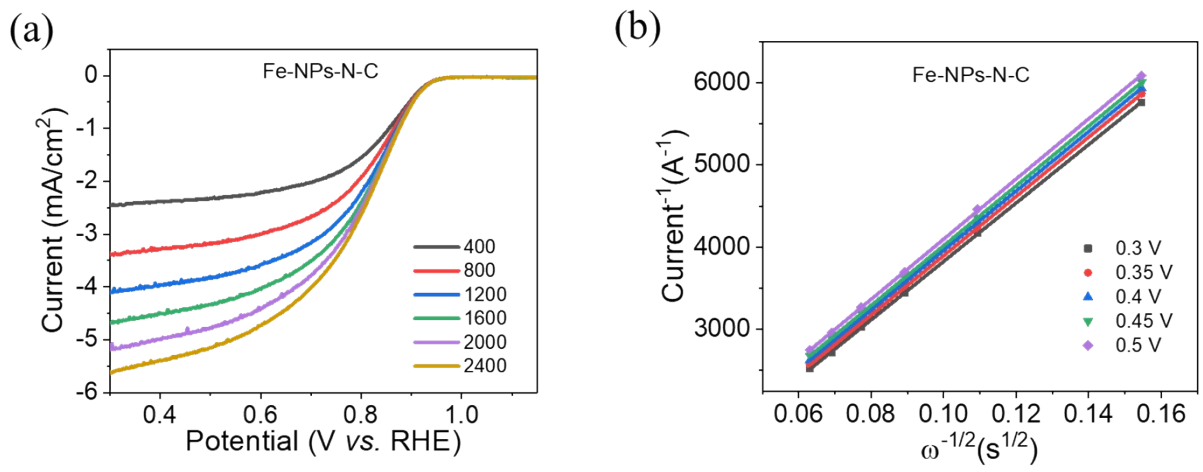

Fig. S8 (a) ORR polarization curves of Fe NPs-N-C recorded at different rotation rates in O_2 saturated 0.1 M KOH with a scan-rate of 10 mV/s, b) the corresponding K-L plots at different potentials *w.r.t.* RHE.

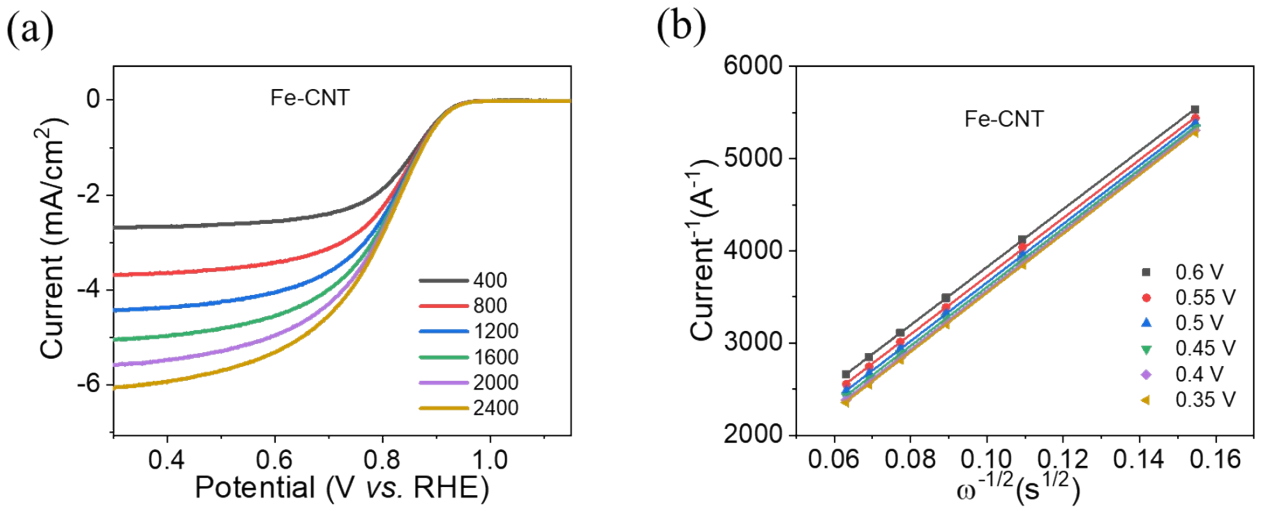

Fig. S9 (a) ORR polarization curves of FeCNT recorded at different rotation rates in O_2 saturated 0.1 M KOH with a scan-rate of 10 mV/s, b) the corresponding K-L plots at different potentials w.r.t. RHE.

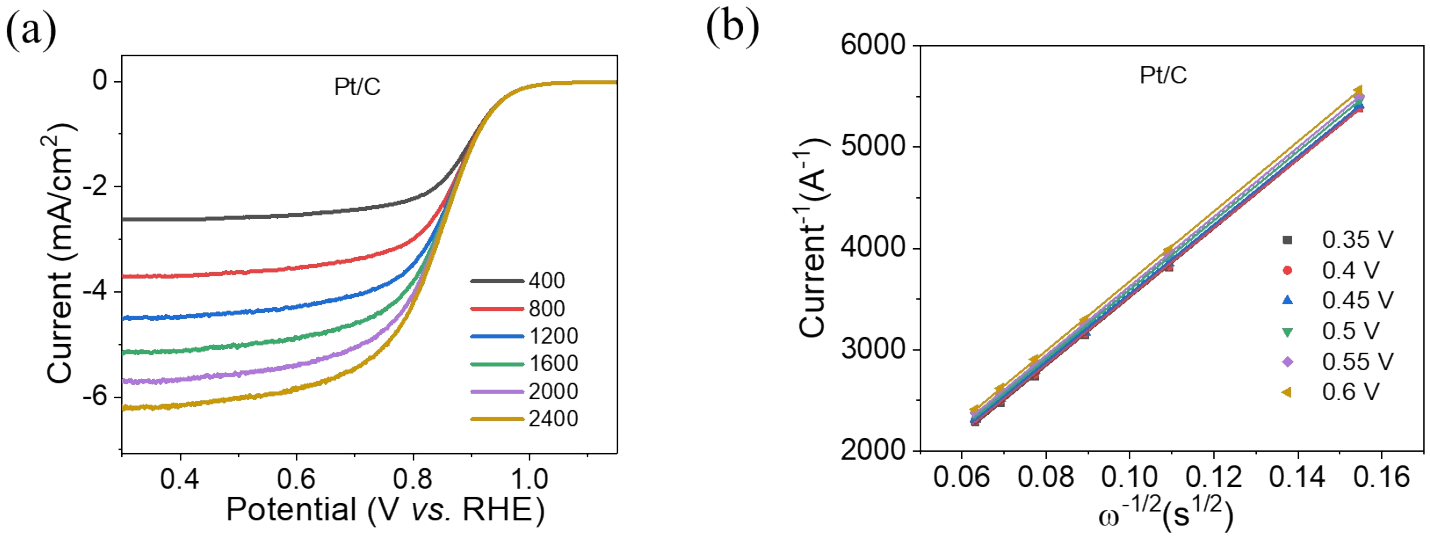

Fig. S10 (a) ORR polarization curves of Pt/C recorded at different rotation rates in O_2 saturated 0.1 M KOH with a scan-rate of 10 mV/s, b) the corresponding K-L plots at different potentials w.r.t. RHE.

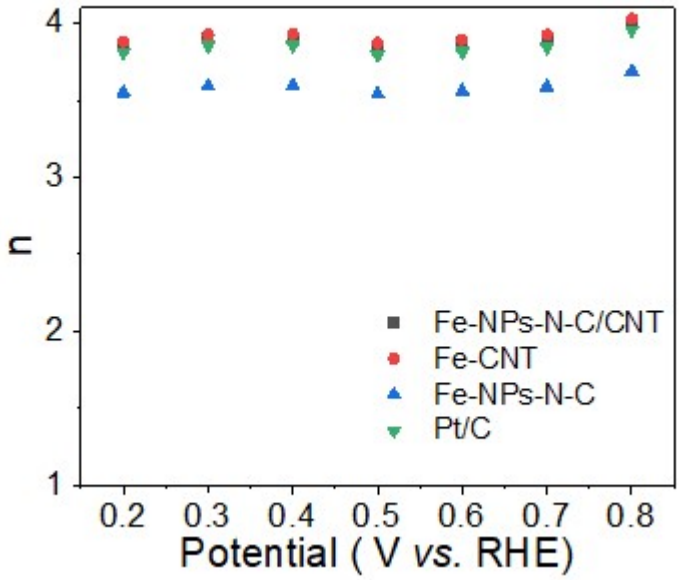

Fig. S11 Plot of electron transfer number *vs*. applied potential w.r.t RHE derived from RRDE measurements.

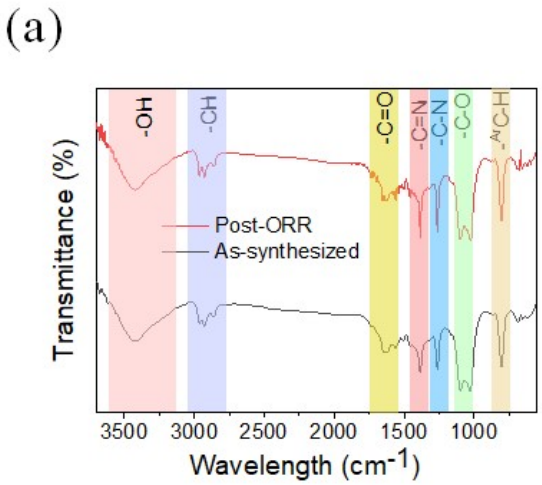

Fig. S12a FTIR spectra of Fe-NPs-N-C/CNT before and after 10,000 CV cycles.

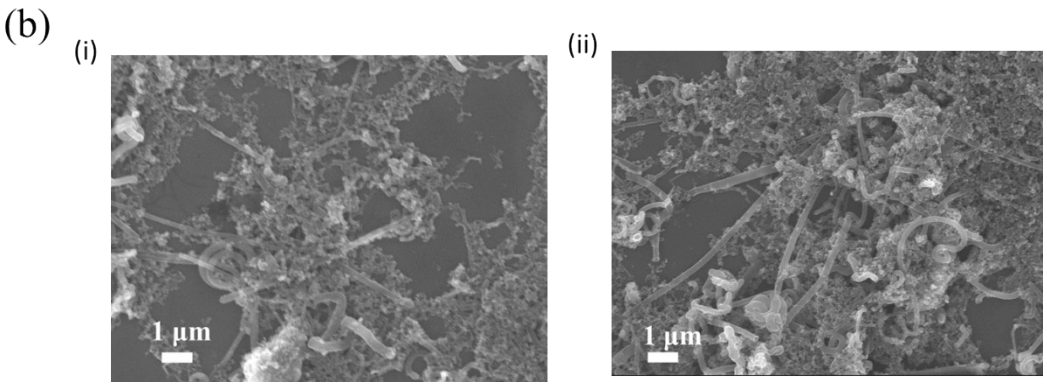

Fig. S12b SEM images of Fe-NPs-N-C/CNT before (i) and after (ii) 10,000 CV cycles.

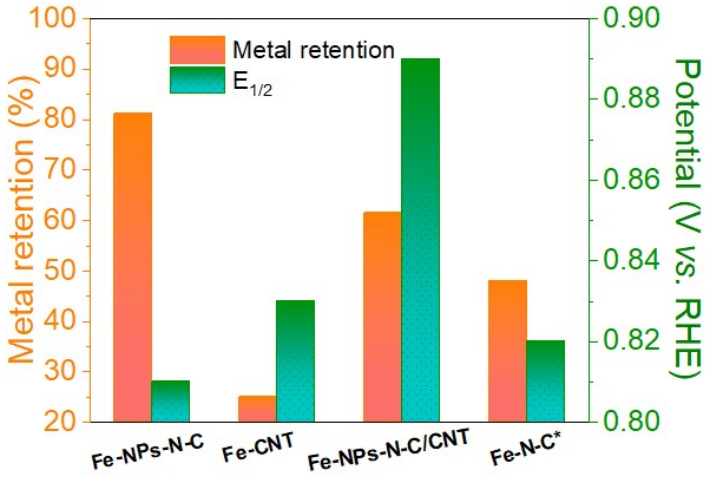

Fig. S13 Plot showing the inverse relationship between metal retention during catalyst preparation and its electrocatalytic activity with an exception for the composite sample (Fe-NPs-N-C/CNT) (* represents the data reported for atomically dispersed Fe on N-C)[4]

S.No.	Electrocatalysts	ORR $E_{1/2}$ (V *vs.* RHE)	Electrolyte	Stability	Reference
1.	**Fe-NPs-N-C/CNT**	**0.89**	**0.1 M KOH**	**Less than 1mV shift in $E_{1/2}$ after 10000 cycles**	**This work**
2.	MN7-10/3 CNT	0.82	0.1 M KOH	Current retained 97.6% after 10000 sec	5
3.	Fe-CNTs/NC	0.84	0.1 M KOH	10% current decrease after 20000 sec	6
4.	N-Fe-CNT/CNP	0.87	0.1 M NaOH	3 mV shift in $E_{1/2}$ after 5000 cycles,	7
5.	Co@NC-ZM	0.83	0.1 M KOH	after 3000 cycles, no change in $E_{1/2}$	8
6.	Fe-CNx/CNT	0.82	0.1 M KOH	5% drop in current after 72000 sec	9
7.	G-Fe/Fe3C-NC/CNTs	0.87	0.1 M KOH	8 mV shift in $E_{1/2}$ after 6000 cycles	10

Table S1 Comparison of ORR performance of Fe-NPs-N-C/CNT with recently reported literature data.

8.	Fe@N-CNTs@rGO	0.83	0.1 M KOH	10 mV shift in $E_{1/2}$ after 3000 cycles	11
9.	Fe/N-CNT-0.1	0.84	0.1 M KOH	96% current retained after 30000 sec	12
10.	Co/N-CNT-750	0.87	0.1 M KOH	3.5% current loss after 25000 sec	13

References

1 G. S. Bang, G. W. Shim, G. H. Shin, D. Y. Jung, H. Park, W. G. Hong, J. Choi, J. Lee, and S. Y. Choi, *ACS Omega,* 2018**, 3,** 5522–5530.

2 C. Zhang, D. M. Dabbs, L. M. Liu, I. A. Aksay, R. Car, and A. Selloni, *J. Phys. Chem. C,* 2015, **119,** 18167–18176.

3 S. Su, L. Huang, S. Su, C. Meng, H. Zhou, L. Zhang, T. Bian and A. Yuan, *ACS Appl. Nano Mater.*, 2020, **3**, 11574–11580.

4 R. Garg, L. Sahoo, K. Kaur, C. P. Vinod and U. K. Gautam, *Carbon*, 2022, **196**, 1001–1011.

5 A. Yu, Z. Peng, Y. Li, L. Zhu, P. Peng and F. Li, *ACS Appl. Mater. Interfaces* 2022, **14**, 42337−42346.

6 L. J. He, J. Q. Zhong, Y. M. Liu, Z. J. Zhou and W. H. Yang, *ChemistrySelect*, 2020, **5**, 12759–12763.

7 H. T. Chung, J. H. Won and P. Zelenay, *Nat. Commun.*, 2013, **4**, DOI:10.1038/ncomms2944.

8 H. Liu, S. Wang, L. Long, J. Jia and M. Liu, *Nanotechnology*, 2021, 32 (20), DOI:10.1088/1361-6528/abe32f.

9 C. Xiao, X. Chen and Y. Tang, *Nanotechnology*, 2017, 28(22), DOI:10.1088/1361-6528/aa6ec3.

10 S. Su, L. Huang, S. Su, C. Meng, H. Zhou, L. Zhang, T. Bian and A. Yuan, *ACS Appl. Nano Mater.*, 2020, **3**, 11574–11580.

11 X. Han, Z. Zheng, J. Chen, Y. Xue, H. Li, J. Zheng, Z. Xie, Q. Kuang and L. Zheng, *Nanoscale*, 2019, **11**, 12610–12618.

12 Y. Gao, T. Li, J. Yang, Y. Zi, X. Zhou and J. Tang, *Mater. Lett.*, 2022, **306**, 130987.

13 D. Zhang, R. Ding, Y. Tang, L. Ma and Y. He, *ACS Appl. Nano Mater.*, 2022, **5**, 10026–10035.